Applied Catalysis B: Environmental 182 (2016) 449–455

Contents lists available at ScienceDirect

Applied Catalysis B: Environmental

journal homepage: www.elsevier.com/locate/apcatb

Environmentally effective photocatalyst CoO–TiO_2 synthesized by thermal precipitation of Co in amorphous TiO_2

A.K.P.D. Savio[a,1], J. Fletcher[a,1], K. Smith[b,1], R. Iyer[b], J.M. Bao[c], F.C. Robles Hernández[a,*]

[a] University of Houston, Department of Mechanical Engineering Technology, College of Technology, 4730 Calhound Rd., Houston, TX 77204-4020, USA
[b] Center for Life Sciences Technology, 385 Technology Building, University of Houston, Houston, TX 77204, USA
[c] Department of Electrical and Computer Engineering, University of Houston, Houston, TX 77204, USA

ARTICLE INFO

Article history:
Received 1 May 2015
Received in revised form
18 September 2015
Accepted 25 September 2015
Available online 30 September 2015

Keywords:
Photocatalysis
Paraoxon
Degradation
Spectroscopy
TiO_2

ABSTRACT

We report the enhanced photocatalytic activity of TiO_2 by the surface decoration of CoO nanoparticles to degrade paraoxon. The CoO nanoparticles are precipitated *in situ* during heat treatments of Co doped amorphous TiO_2 and enhance the degradation by 11–24 times that of pure TiO_2 or Rh_2O_3–TiO_2 or the oxide nanoparticles under white light (natural sunlight and fluorescence light). The enhanced activity is a combined result of visible light absorption by CoO and effective electron-hole separation at the CoO–TiO_2 interfaces.

Published by Elsevier B.V.

1. Introduction

Titanium-dioxide (TiO_2) is often used for photocatalysis to degrade organic and biological substances [1–5] due to its stability and cost. TiO_2 is not efficient in sunlight limiting its use under UV irradiation, which accounts for 5% of solar spectrum. There have been various approaches to improving visible light response of TiO_2, for example, by attaching photosensitizers to TiO_2 surfaces, doping (bandgap reduction), induce new states within the bandgap [6–8]. Photosensitizers suffer from photo corrosion and are not as stable as TiO_2. Although doped TiO_2 can operate in the visible region, but its photocatalytic activity is far lower than that of unmodified TiO_2 under UV irradiation. Furthermore, doping can also reduce the activity of TiO_2 under UV irradiation because the doped species could act as recombination centers [7,9,10]. In recent years we demonstrated the effectiveness of sonosynthesis to prepare pure and doped TiO_2 [10–12]. The use of pure TiO_2 for water purification and the removal of pesticides (*e.g.*, paraoxon and p-nitrophenol) has been previously demonstrated [4,13–15]. Here we demonstrate that CoO–TiO_2 is photocatalytically active using sunlight or fluorescent light instead of ultraviolet light.

The chemical paraoxon, an organophosphate, is a potent neurotoxin and has been extensively used as an insecticide. Most organophosphorus pesticides are vinyl ester derivatives of phosphates and have been widely used as insecticides and chemical warfare agents [16] that has accumulate in the soil and it is now a major health concern [17]. The organophosphates are cholinesterase inhibitors and irreversibly bind to acetylcholinesterase (AChE) and rendering it inactive [18]. Inactive AChE prevents the degradation of acetylcholine can quickly kill by causing convulsions, brain seizures, respiratory failure etc. [18,19]. Several methods have been used to destroy these toxic compounds, including chemical hydrolysis, incineration and microbial enzymatic degradation by microbial enzymes [20,21].

In the present work is demonstrated a new catalyst that has enhanced efficiency when compared to pure TiO_2. This enhancement is the result of the precipitation (decoration) of nanoparticles (*e.g.*, CoO) on the surface of TiO_2. Metallic cations are added as dopants (Co and Rh) and they precipitate in amorphous TiO_2 during the synthesis. The novelty presented herein is the use of heat treatments to promote "back-diffusion" of the cations allowing to control the particle size within the nanometric range (CoO or Rh_2O_3). A variety of nanostructure precipitates are used to enhance the photo-catalytic efficiency of TiO_2; yet, CoO seem to be the most effective. The photocatalytic degradation of paraoxon is used as

* Corresponding author. Fax: +1 505 213 7106.
E-mail address: fcrobles@uh.edu (F.C. Robles Hernández).
[1] Authors with similar contribution.

http://dx.doi.org/10.1016/j.apcatb.2015.09.047
0926-3373/Published by Elsevier B.V.

standard benchmark reaction to demonstrate the enhancement benefits CoO nanoparticles on TiO_2.

We have chosen paraoxon as a benchmark and for its known resistant to degradation. At the current state we do not propose our photocatalyst as a solution for soil treatment or remediation; instead, we are demonstrating that CoO nanoparticle decorated TiO_2 are highly effective in the absence of intense UV light and may result effective for fresh water sources (*e.g.*, rivers, lakes, water treatment, etc.). We also show our unique method to synthesize such hybrid catalyst.

2. Experimental

2.1. Catalyst synthesis

The chemicals used in the present work are described in Table 1, and a complete list of chemicals to produce all catalysts tested is provided in the supplementary material (SM). We tested the following catalysts: pure TiO_2, Al–TiO_2, C–TiO_2, CoO–TiO_2, α-Fe_2O_3–TiO_2, and Rh_2O_3-TiO_2; but in the interest of brevity the main text focuses only TiO_2, CoO–TiO_2, and Rh_2O_3–TiO_2. The stoichiometry of the nanoparticles that decorate TiO_2 is taken from our previous work [22]. For the sonosynthesis De-ionized water (30 ml) is added drop wise to 150 ml of titanium isopropoxide ($Ti[OCH(CH_3)_2]_4$) during sonication. The temperature in the sonicator is set to 40 °C via water cooling. The dopant agents are dosed separately from water; however, they are added through the synthesis to secure its integration with TiO_2.

The results presented here correspond to pure TiO_2 and with 0.1 at% additions of Co, or Rh. The sonication was assisted by a Misonix S-2000 apparatus operated with micro-tip using amplitude of 100%, 20 kHz for 30 minutes delivering 25 j/s. The resulting colloid was dried on a hot plate at 60 °C for 24 hours. The dry powders are TiO_2 with organic residue; the drying step is concluded when the powder attains a loose appearance. The organic residue is removed by deionized water wash, which is repeated 10 times. Each wash is accompanied by a draining procedure performed via micropore filter paper on a funnel-flask with an applied vacuum pump. The powders are dried a final time before they are heat treated.

2.2. Heat treatment

The heat treatments were monitored via thermal analysis using a workstation consisting of a high-speed-high-resolution National Instruments data acquisition system (cFP 1804, Austin, TX) and a personal computer set to 10 readings per second. The pure TiO_2, Co–TiO_2 and Rh–TiO_2 were heat treated at 300 and 800 °C for 12 h in a tube electric resistance furnace in open air conditions.

2.3. Characterization

The XRD characterization was conducted on a SIEMENS Diffractometer D5000 equipped with a Cu target; the Kα characteristic has a $\lambda = 0.15406$ nm. The scanning electron microscopy (SEM) observations were carried out on a FEI XL-30FEG in secondary electrons mode. The samples were prepared by depositing the powders on graphite tape and coating with gold. High Resolution Transmission Electron Microscopy (HRTEM) was conducted on a JEOL 2000 FX operated at 200 kV and the samples were done adding a pinch of powder onto 3 ml of ethanol that was sonicated for 1 min followed by sedimentation until the liquid is clear. Two drops of the suspension were deposited on a Cu grid (300 mesh).

Raman spectroscopy was conducted on an XploRA^{TM} apparatus using a green laser (532 nm) with a spot size is 1 μm and a resolution of 0.5 cm^{-1}. UV–vis was conducted to obtain the bandgap that was calculated using a modified Kulbeka–Munk method [23]. The samples for Raman and optical spectroscopy were prepared by adding 0.01 g of powder in 20 ml of de-ionized water. The mix was subjected to sonication for 10 min using an intensity of 25 j/s. The resulting suspension was deposited on fused silica glasses (4 mm in diameter) that were dried on a hot plate at 60 °C for 2 h. The process was repeated 5 times to thicken the films. Pictures of the sonicated suspension (water-catalyst) are presented in the SM1 showing that the catalyst can be suspended on water for 8 h or more. The amounts of catalyst for the degradation test and for the samples used for the UV–vis test may vary; nonetheless, we can confirm that some of the catalyst is suspended during the degradation test.

2.4. Catalytic degradation of paraoxon

The catalysts were tested the degradation of the organophosphate compound paraoxon into the by-product p-nitrophenol (PNP) under two lighting conditions: (i) natural sunlight and (ii) fluorescent light. The spectra for both, are included in the SM 2. The samples were prepared in sterile 14 mL falcon tubes with 10 mL of sterile carbon supplemented media (CSM). The selection of the minimal media CSM as a resuspension agent follows the experimental method previously employed by Iyer et al. [24,25] where the concentration of paraoxon is measured by means of UV–vis. This is a well established method that we have been using for several years and was reported in our previous publications [24,25]. The amount of catalyst added in every case was 0.5 g. The concentration of paraoxon was 100 μg per mL of CMS for a final concentration of 2 mg of paraoxon/gram of catalyst. The tubes were then sealed and vortexed for approximately 10 s. The vortex time sufficient to suspend the catalyst; although, some particles may precipitate.

For the sunlight lighting conditions, the sample tubes were placed on a bench top adjacent to an exterior facing window (sunlight spectra is available in the SM 2a). The fluorescent light was carried in a close container to isolate any interaction with sunlight or any other source. The light spectra for the fluorescent source is available in SM 2b. The temperature during the procedures was remained constant at approximately 29 °C for both lighting conditions.

For the degradation analysis a 500 μL aliquot was collected from each tube at designated times from Day 0 to Day 6 (approx. 144 h). Each time an aliquot is taken, the remaining sample is vortexed again to ensure that the catalyst is suspended again for the rest of the test. The aliquot was centrifuged at 13,400 rpm for 2 min at room temperature; the supernatant was read at 200 μL per well, in duplicate, by plate spectrophotometry in a wide spectrum scan between 230 and 1000 nm by Tecan UV–vis plate spectrophotometer.

3. Results

3.1. Materials: synthesis and characterization

Fig. 1 shows characterization of pure TiO_2 and with Co and Rh additions in the as synthesized and heat treated conditions using SEM, XRD, and Raman spectroscopy. The grain size was calculated using the Sherrer method [26,27]. For the three samples in the as synthesized conditions the grain is sub-nanometric, hence quasi-amorphous and this is in agreement with Fig. 1d. On the other hand, for the pure TiO_2 and with Co or Rh additions for the heat treated samples between 300 and 800 °C for 12 h the grain sizes vary from 1.5 to 5 nm respectively (Fig. 1e–f). Thermal analysis results demonstrate that using sonochemistry the crystallization of the powders to anatase occurs at relatively low temperatures (*e.g.*, 100 °C [11]). The diffraction pattern for pure TiO_2 heat treated

Table 1
Chemical agents used in the present work with their respective purity and vendors.

Name	Formula	Purity(wt%)	Vendor
Titanium isopropoxide	$Ti[OCH(CH_3)_2]_4$	97.00	Sigma–Aldrich
Agents			
Cobalt (III) Fluoride	CoF_3	99.99	Sigma–Aldrich
Rhodium (III) nitrate ~36wt% rhodium	$Rh(NO_3)_3$	99.99	Sigma–Aldrich
Paraoxon (pesticide)			
Paraoxon	$O_2NC_6H_4OP(O)(OC_2H_5)_2$	98.9	Supelco
Acetonitrile	C_2H_3N	99.5	Fluka
CSM: Carbon Selective	De-ionized water	94.5 mL	
Media (prepared in lab,	1 M NTA	200 uL	Sigma–Aldrich
sterilized by autoclave)	20% (w/v) $MgSO_4$ $7H_2O$	100 uL	Sigma–Aldrich
	4% (w/v) $Ca(NO_3)_2$		
	0.5% (w/v) $FeSO_4$ $6H_2O$	100 uL	Sigma–Aldrich
	Phosphate Buffer	100 uL	Sigma–Aldrich
	Solution (Stock solution)	5 uL	Sigma–Aldrich

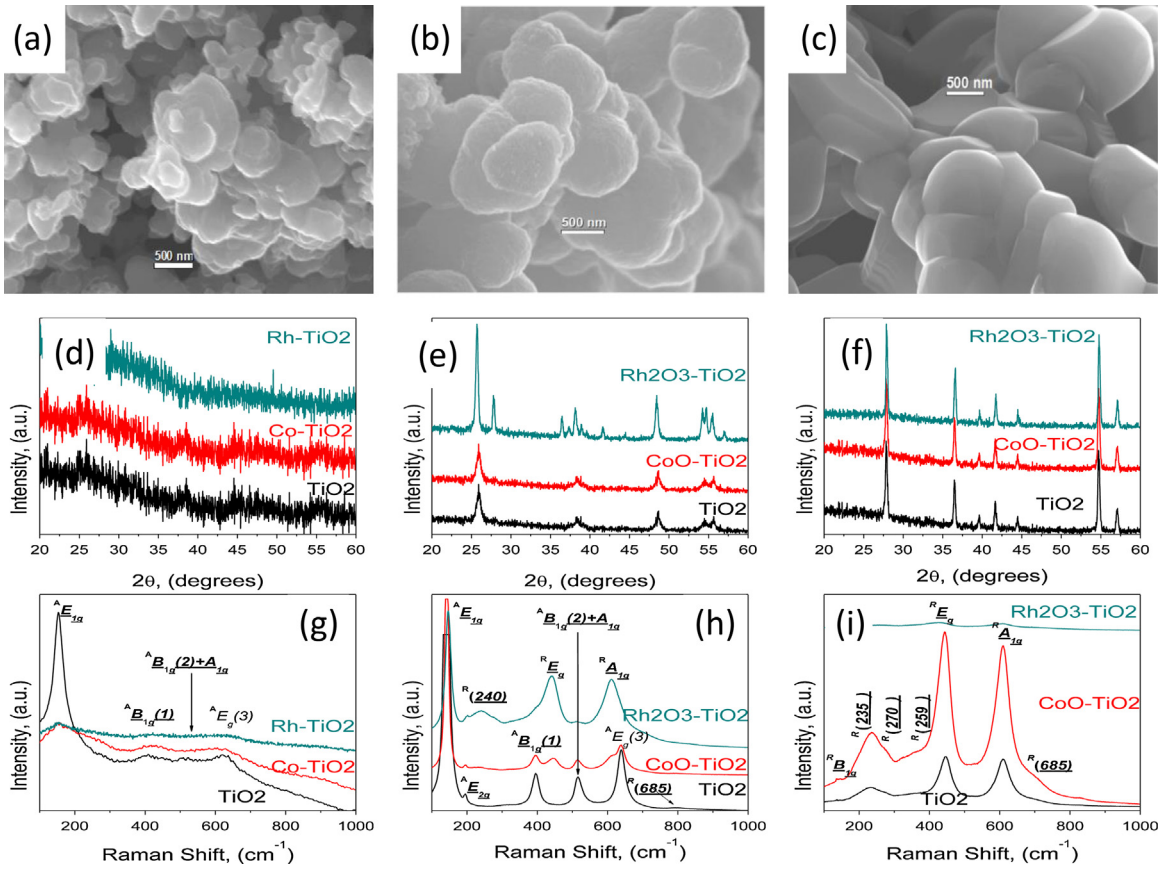

Fig. 1. Characterization of the as synthesized and heat treated samples by means of (a–c) SEM, (d-f) XRD and (g–i) Raman Spectroscopy. The results correspond to the samples in the following conditions: (a,d,g) As synthesized samples, (b,e,h) samples heat treated at 300 °C and (c,f,i) samples heat treated at 800 °C. Note: In the Raman spectrum the upper left letters (A or R) denote anatase or rutile respectively.

at 300 °C shows the presence of pure anatase. The phase transformation observed during the heat treatments are in agreement with references [28–30].

The transformation to rutile is initiated above 300 °C and completes above around 500 °C, but this also depends on the additions (*e.g.*, Co, Rh) [11,31]. The heat treated sample (CoO–TiO_2) at 300 °C is mainly anatase with 5 ± 2 wt% rutile. The Rh_2O_3-TiO_2 sample has approximately 70 ± 5 wt% anatase and up to 30 ± 5 wt% rutile. Therefore, we can say that both, Co and Rh, are rutile promoters, and Rh is more effective.

The samples heat treated at 800 °C possess higher crystallinity and in all cases are pure rutile (Fig. 1f); unfortunately, the particles are coarser. Therefore, we decided to use the materials heat treated at 300 °C because they allow proper crystallization of TiO_2, but prevent undesirable coarsening. At the same time with this heat treatment it is possible to synthesize key cobalt and rhodium oxides semi-conductors with unique co-photocatalyst enhancement. This is a unique process where the TiO_2 is decorated with effective co-photocatalytic particles of CoO or Rh_2O_3.

Fig. 1a–c are SEM images for the as synthesized and heat treated materials respectively. The SEM micrographs indicate the coarsening evolution for pure TiO_2 and the densification effects by the higher temperature during heat treatment. The particle growth during coarsening goes from irregular into faceted with sharp

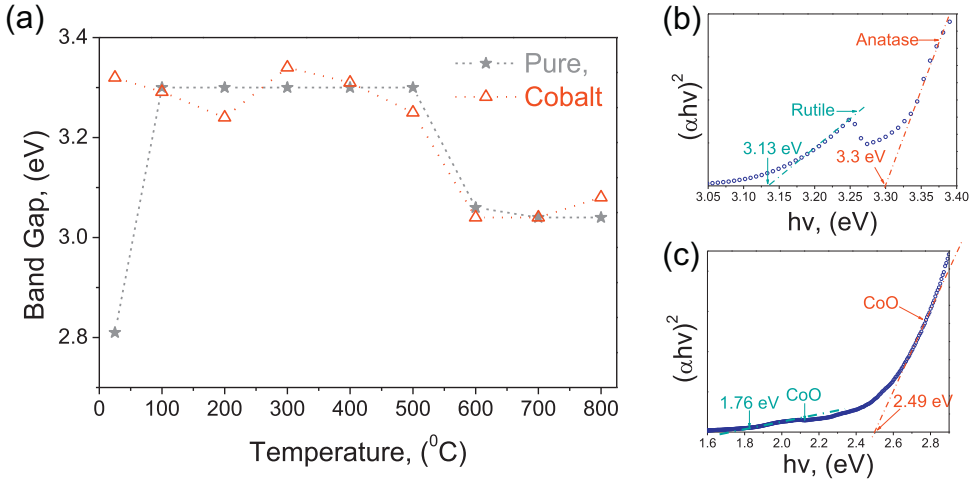

Fig. 2. Bandgap results of the (a) as synthesized and heat treated TiO_2 with Co additions. The Figures in (b–c) are the bandgap results for (b) pure TiO_2 heat treated at 500 °C and (c) CoO–TiO_2 heat treated at 800 °C. Notice in (b and c) are shown more than one bandgap that is due to the presence of multiple phases typical of TiO_2 and CoO.

edges implying higher crystallinity with reduced surface area. The irregular appearance in the as synthesized TiO_2 is attributed to incompleted stoichiometries and potentially a lack of oxygen. Again, this implies that the best candidate if the material heat treated at 300 °C.

The Raman characterization of the heat treated samples for as synthesized CoO–TiO_2 shows an intense $E_{g(2)}$ band. This band is well resolved due to a short to mid-range order [11]. Other identifiable Raman bands (Fig. 1g-i) for anatase are: E_g, B_{1g}, and the doublet A_{2g}. The E_g mode shows three bands at 151, 193 and 630 cm^{-1}, while the B_{1g}, A_{1g} and B_{1g} are at 400, 508 and 512 cm^{-1} respectively [32]. When anatase is nanostructured the E_g band (144 cm^{-1}) shows a red shift, based on the results from [33,34]; the grain size in our materials is 5 nm that is in agreement with XRD results. The as synthesized Rh_2O_3-TiO_2 sample is almost amorphous; we cannot calculate its grains size and we can only assume that is smaller than that in CoO–TiO_2 (Fig. 1d).

All heat treated samples exhibit second order Raman scattering at about 240 cm^{-1} and a shoulder at around 685 cm^{-1} that are typical of rutile [35]. The CoO–TiO_2 sample fully transforms into rutile when heat treated at 800 °C and is confirmed with the Raman bands that are identical to those reported in [35]. The Raman intensity in Rh_2O_3–TiO_2 heat treated at 800 °C decreases considerably due to the surface decoration of the Rh_2O_3 precipitated along the TiO_2 particles. The Rh_2O_3 blocked laser beam, preventing the identification of TiO_2. Yet, XRD clearly identifies the TiO_2 as pure rutile with the following lattice parameters: $a = 0.459$ and $c = 0.295$ nm that are similar to those reported in [36]. Here is important to clarify that the Co and Rh additions are dopants in the as synthesized (amorphous) samples, but during the heat treatment they form oxide precipitates that decorate TiO_2.

Fig. 2 illustrates the bandgap values for the TiO_2 and CoO–TiO_2 samples. The values reported for the bandgap in the as synthesized TiO_2 is comparable to that in our previous work (2.8 eV [11]) that is evidently lower than that presented in commercial sources (3.0–3.2 eV [37]). This difference is due to incomplete stoichiometries. Similar results have been reported in rutile/anatase heterojunctions with values of 2.78 eV [38], but in our case we attribute this change to dangling bonds and in samples above 500 °C show only the bandgap for rutile (3.1 eV).

The CoO–TiO_2 has three absorption bands (Fig. 2c). One of those corresponds to TiO_2 and the other two are for CoO. The respective bandgap analysis is given in Fig. 2c. The two bandgap values at 1.71 ± 0.04 eV and 2.45 ± 0.05 eV match those reported previously for CoO [39]. In the Rh_2O_3–TiO_2 sample we also identified more than one bandgap (2.38 and 2.7 eV) for Rh_2O_3 that are comparable to those reported in the literature. [40]. Again, the presence of the Rh_2O_3 nanoparticles prevented the precise determination of the bandgap on TiO_2, which we assume is identical to that shown in Fig. 2 for pure TiO_2.

3.2. Catalysis: chemical principles

Fig. 3 shows the degradation sequence of paraoxon by the catalytic effect of TiO_2. The degradation is initiated when the paraoxon is decomposed into the p-nitrophenol and diethyl phosphate (DEP). This degraded species are important due to their limited toxicity that is two orders of magnitude less than paraoxon [41]. Here

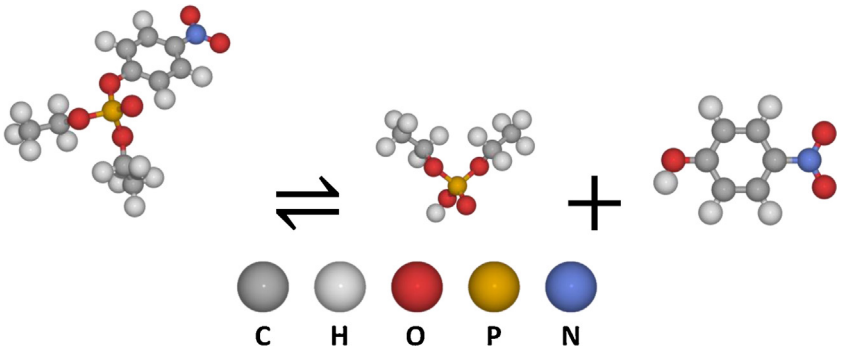

Fig. 3. Sketch of the chemical degradation of paraoxon on to o,o-diethylphosphate + p-nitrophenol by the catalytic effect of the doped TiO_2.

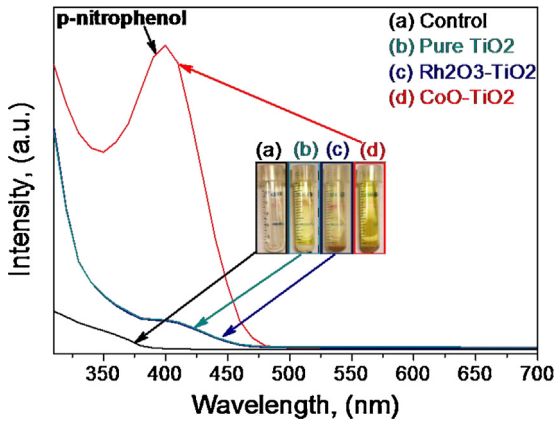

Fig. 4. Catalytic degradation of paraoxon using various catalyst and a control sample. The efficiency of the Co-TiO_2 is clearly evident when compared to the other tested samples, the experiment presented herein was carried for 1 day under sunlight conditions. Furthermore, the control sample do not show evidence of the degraded species.

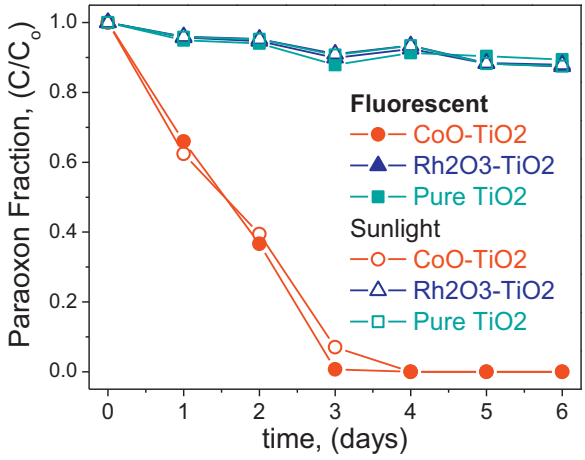

Fig. 5. Results of photocatalytic degradation of paraoxon using pure TiO_2, CoO–TiO_2, and Rh_2O_3–TiO_2 for duration between 1 and 6 days.

we investigate the rate of paraoxon degradation by the directly correlated spectroscopic quantification of p-nitrophenol. The p-nitrophenol is further degraded into p-benzoquinone [13,42–44].

3.3. *Catalysis: degradation of paraoxon*

The initial experiment deomonstrated that using a concentration of 2 mg of paraoxon/gram of catalyst was ideal to carry the test presented herein.

Fig. 4 shows the UV–vis absorbance curves indicating the degradation efficiency for various catalysts after 1 day of test under sunlight conditions. The degradation detection is conducted by analyzing the degraded species as shown in Fig. 4, which is identified as p-nitrophenol at approximately 400 nm. The second degree of degradation is p-nitrophenol transform into p-benzoquinone as reported in our previous work [24,25]. It is important to notice that after the first day the most active catalyst is CoO-TiO_2, the pure TiO_2 and Rh_2O_3–TiO_2 have comparable degradation activity. The control sample does not seem to have any presence of p-nitrophenol as expected.

In Fig. 5 shows clear catalytic enhancement of CoO–TiO_2 over pure TiO_2 and Rh_2O_3–TiO_2. The difference is enough to degrade paraoxon into p-nitrophenol. In addition, both lightening conditions, sunlight and fluorescent, seem to have comparable degradation effects on paraoxon. In the first day, under sunlight 37% of paraoxon is degraded and for the fluorescent light conditions the degradation is 36%. By the second day the corresponding degradation values are 60.5% and 63.5%. In the third day of testing the fluorescent experiment degrades 99.9% of paraoxon and with sunlight it is 97%. The presence of paraoxon in the fourth day is untraceable.

On the other hand, pure TiO_2 and Rh_2O_3–TiO_2 have comparable efficiencies; however, after 6 days of exposure the degradation reaches only from 11 to 13%. For pure TiO_2 and Rh_2O_3–TiO_2 the fluorescent conditions seem more effective; nonetheless, when compared to CoO–TiO_2 this difference is almost negligible. Under fluorescent light, the degradation of paraoxon is 11.5 times faster for CoO–TiO_2 than the other catalyst. In the presence of sunlight this difference increases to 13 and 16 times with respect to Rh_2O_3–TiO_2 and pure TiO_2. Therefore, CoO–TiO_2 is the most effective photocatalytic compound tested herein. For other catalyst compounds the results are presented in SM 4. The use of CoO–TiO_2 degrades the p-nitrophenol into p-benzoquinone. The presence of p-benzoquinone is detected after the first day of test. After the fifth day the presence of p-nitrophenol is untraceable. This degradation is not clear for pure TiO_2 or Rh_2O_3.

Larger amounts of CoO-TiO_2 were also tested. Increasing the concentration of CoO-TiO_2 catalyst to 1.25 mg of paraoxon/gram we observe that paraoxon degrades completely in approximately 27 h under fluorescent light; however, under sunlight the degradation is only 67%. The degradation activity of CoO-TiO_2 under fluorescent light is 265% with an extra addition of 62.5% of catalyst (from 0.5 to 0.8 g). In other words, 0.8 g of CoO-TiO_2 per mg of paraoxon can complete the photocatalytic degradation approximately 24 times faster than pure TiO_2 that is equivalent to 2400% improvement.

4. Discussion

The Pt- and Rh-additions to TiO_2 are usually reported as effective dopants to enhance photocatalyst efficiency [45]. This is somehow explained by the effectiveness of those noble metals to narrow the bandgap in TiO_2 when it is present as a dopant. However, in the present work we demonstrated that CoO–TiO_2 is more efficient than Rh_2O_3–TiO_2. This higher effectiveness of the CoO-TiO_2 is due to a co-photocatalytic property of CoO [46].

The CoO and $Rh2O_3$ are decorating the TiO_2 particles, which resulted as a side effect of the heat treatment due to a precipitation of Co or Rh cations that are forced out of TiO2 due to a "back-diffusion" mechanism as suggested in our previous publication [11]. The main advantage of this method is the controlled precipitation and coarsening of oxide nanoparticles. The heat treatments are designed to precipitate pure CoO avoiding coarsening. The presence of CoO is identified and confirmed by Raman, UV–vis (bandgap) and HRTEM. The presence of CoO on TiO_2 is clear in the HRTEM results in Fig. 6. The additions of Co and Rh were used to engineer nanostructured TiO_2 particles decorated with oxide catalyst that resulted in clear enhancements of the photo-catalytic activity when compared to pure TiO_2.

The high activity of CoO–TiO_2 under visible light makes it suitable for environmental applications. Furthermore, the CoO-TiO_2 is the only catalyst that is able to complete a secondary degradation from p-nitrophenol into p-benzoquinone [13,42,43]. The second best photocatalyst is the α-Fe_2O_3–TiO_2 (see SM 4) that reaches 77% of degradation after 6 days. In comparison, only 11% and 12% of paraoxon was degraded in the same time by Rh_2O_3-TiO_2 or TiO_2 respectively.

Co is significantly more affordable than Rh or other precious metals. Other examples in the literature to degrade organics with TiO_2 using light sources in all cases with intense UV component

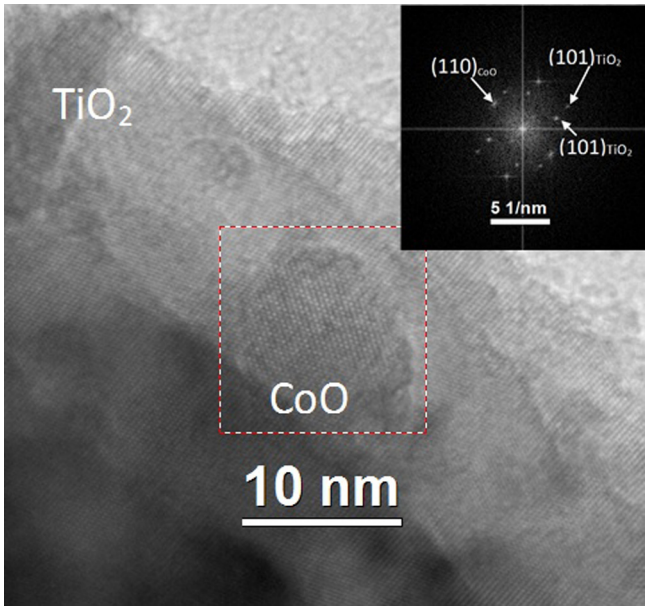

Fig. 6. The HRTEM of the CoO-TiO_2 showing the "substrate" of TiO_2 "decorated" by a particle of CoO (doted square). The insets on the right upper corner shows the FFT of the dotted square region showing a dual patter further confirming the presence of both phases (CoO and TiO_2).

(200–340 nm), elevated temperatures (60–80 °C) and light sources that are 25 times or more intense [2,47] when compared to the light sources used herein. It is certainly true that the complete degradation is faster on other reports (*e.g.* literature); yet our procedure is effective in the absence of special light sources. Therefore, our process is environmentally friendly (sunlight, room temperature and atmospheric pressure). Our environmentally friendly process is probably not ready for soil remediation because the soil may block the light (except at the surface); yet, it can be considered for fresh water treatment in isolated systems (*e.g.*, photoreactors). It means, before the water is returned into rivers, lakes, etc. This is suggested to avoid health and pollution concerns known in cobalt. If external lightening is needed our catalyst can easily work with city light sources (fluorescent) avoiding intense UV light typically used in laboratory set-ups and confined spaces due to its health restrictions [2,47]. Because our process is effective at room temperature we can realistically say that this is the only possible way to carried it environmentally.

5. Conclusions

In this work it is demonstrated that paraoxon can be effectively degraded to less toxic substances using CoO–TiO_2. Only 0.1 at% of Co is enough to develop the needed photocatalytic effect on TiO_2 to make it effective under sunlight. The CoO are particles that precipitate *in situ* during heat treatment of Co doped amorphous TiO_2. The CoO exhibits a co-photocatalytic activity that enhances TiO_2 organic degradation. The CoO and Rh_2O_3 nanoparticles have sizes of 5 nm or less that are key to generate the co-catalytic effect. Among all the tested photocatalysts the CoO–TiO_2 is the most effective and it is active under environmentally friendly conditions (temperature, sunlight, pressure, etc.) reaching degradation activies of up to 16 times that of pure TiO_2. It is also proven that p-nitrophenol is further degraded into p-benzoquinone in a secondary degradation breaking the original molecule into a significantly less harm one.

Acknowledgements

The authors would like to thank the University of Houston and the State of Texas for their invaluable support through the Star Up, Small grant and HEAFS funding. The authors would like to thank Dr. L. Grabow and Mr. H. Doan for the molecular models in Fig. 3 as well as the highly educated comments in this manuscript. J.M.B acknowledges support from the Robert A. Welch Foundation (E-1728).

Appendix A. Supplementary data

Supplementary data associated with this article can be found, in the online version, at http://dx.doi.org/10.1016/j.apcatb.2015.09.047.

References

[1] J.K. T.S. Kim, K. Kim, M.K. Choi, K.D. Zoh Stenstrom, Degradation mechanism and the toxicity assessment in TiO2 photocatalysis and photolysis of parathion, Chemosphere 62 (2006) 926–933.
[2] G.K. Prasad, P.V.R.K. Ramacharyulu, J.P. Kumar, A.R. Srivastava, B. Singh, Photocatalytic degradation of paraoxon-ethyl in aqueous solution using titania nanoparticulate film, Thin Solid Films 520 (2012) 5597–5601.
[3] H. Chen, M. Shen, R.W. Chen, K. Dai, T.Y. Peng, Photocatalytic degradation of commercial methyl parathion in aqueous suspension containing La-doped TiO_2 nanoparticles, Environ. Technol. 32 (2011) 1515–1522.
[4] L.X. Yang, S.L. Luo, Y. Li, Y. Xiao, Q. Kang, Q.Y. Cai, High efficient photocatalytic degradation of p-nitrophenol on a unique Cu_2O/TiO_2 p-n heterojunction network catalyst, Environ Sci Technol 44 (2010) 7641–7646.
[5] K. Nagaveni, G. Sivalingam, M.S. Hegde, G. Madras, Photocatalytic degradation of organic compounds over combustion-synthesized nano-TiO_2, Environ. Sci. Technol. 38 (2004) 1600–1604.
[6] S.Y. Lee, S.J. Park, TiO_2 photocatalyst for water treatment applications, J. Ind. Eng. Chem. 19 (2013) 1761–1769.
[7] M.A. Lazar, S. Varghese, S.S. Nair, Photocatalytic water treatment by titanium dioxide: recent updates, Catalysts 2 (2012) 572–601.
[8] M.R. Hoffmann, S.T. Martin, W.Y. Choi, D.W. Bahnemann, Environmental applications of semiconductor photocatalysis, Chem. Rev. 95 (1995) 69–96.
[9] U. Diebold, The surface science of titanium dioxide, Surf. Sci. Rep. 48 (2003) 53–229.
[10] F.C. Robles Hernandez, L. Gonzalez-Reyes, I. Hernandez-Perez, Effect of coarsening of sonochemical synthesized anatase on BET surface characteristics, Chem. Eng. Sci. 66 (2011) 721–728.
[11] A.K.P.D. Savio, J. Fletcher, F.C. Robles Hernández, Sonosynthesis of nanostructured TiO_2 doped with transition metals having variable bandgap, Ceram. Int. 39 (2013) 2753–2765.
[12] L. Gonzalez-Reyes, I. Hernandez-Perez, F.C.R. Hernandez, H.D. Rosales, E.M. Arce-Estrada, Sonochemical synthesis of nanostructured anatase and study of the kinetics among phase transformation and coarsening as a function of heat treatment conditions, J. Eur. Ceram. Soc. 28 (2008) 1585–1594.
[13] J. Senthilnathan, L. Philip, Removal of mixed pesticides from drinking water system using surfactant-assisted nano-TiO_2, Water Air Soil Pollut. 210 (2010) 143–154.
[14] J. Senthilnathan, L. Philip, Removal of mixed pesticides from drinking water system by photodegradation using suspended and immobilized TiO_2, J. Environ. Sci. Health B 44 (2009) 262–270.
[15] D. Chen, A.K. Ray, Photodegradation kinetics of 4-nitrophenol in TiO2 suspension, Water Res. 32 (1998) 3223–3234.
[16] S.A. Kardos, L.G. Sultatos, Interactions of the organophosphates paraoxon and methyl paraoxon with mouse brain acetylcholinesterase, Toxicol. Sci. 58 (2000) 118–126.
[17] M. Maroni, A. Fait, Health effects in man from long-term exposure to pesticides. A review of the 1975–1991 literature, Toxicology 78 (1993) 1–180.
[18] S. Singh, N. Sharma, Neurological syndromes following organophosphate poisoning, Neurol. India 48 (2000) 308–313.
[19] X.H. Xu, A.B. Dailey, E.O. Talbott, V.A. Ilacqua, G. Kearney, N.R. Asal, Associations of serum concentrations of organochlorine pesticides with breast cancer and prostate cancer in US adults, Environ. Health Perspect. 118 (2010) 60–66.
[20] C.F. Wu, H.J. Cha, J.J. Valdes, W.E. Bentley, GFP-visualized immobilized enzymes: degradation of paraoxon via organophosphorus hydrolase in a packed column, Biotechnol. Bioeng. 77 (2002) 212–218.
[21] K. Saffih-Hdadi, L. Bruckler, E. Barriuso, Modeling of sorption and biodegradation of parathion and its metabolite paraoxon in soil, J. Environ. Qual. 32 (2003) 2207–2215.
[22] A. Savio, J. Fletcher, F. Robles Hernández, Sonosynthesis of nanostructured TiO_2 doped with transition metals having variable bandgap, Ceram. Int. 39 (2013) 2753–2765.

[23] M.A. Zanjanchi, H. Noei, M. Moghimi, Rapid determination of aluminum by UV–vis diffuse reflectance spectroscopy with application of suitable adsorbents, Talanta 70 (2006) 933–939.
[24] R. Iyer, K. Smith, B. Kudrle, A. Leon, Detection and location of OP-degrading activity: a model to integrate education and research, New Biotechnol. 32 (2015) 403–411.
[25] R. Iyer, V.G. Stepanov, B. Iken, Isolation and molecular characterization of a novel p*seudomonas putida* strain capable of degrading organophosphate and aromatic compounds, Adv. Biol. Chem. 3 (2013) 564–578.
[26] H.P. Klug, L.E. Alexander, X-ray Diffraction Procedures for Polycrystalline and Amorphous Materials, 2d ed., Wiley, New York, 1974.
[27] B.D. Cullity, Elements of X-ray Diffraction, 2nd ed., Addison-Wesley Pub. Co., Reading, Massachusetts, 1978.
[28] F.C. Robles Hernandez, J.H. Sokolowski, Thermal analysis and microscopical characterization of Al–Si hypereutectic alloys, J. Alloy Compd. 419 (2006) 180–190.
[29] F.C. Robles Hernandez, J.H. Sokolowski, Effects and on-line prediction of electromagnetic stirring on microstructure refinement of the 319 Al-Si hypoeutectic alloy, J. Alloy Compd. 480 (2009) 416–421.
[30] F.C. Robles Hernandez, J.A. Neal, U.S. Aldea, Thermal characterization of poultry for the development of a comprehensive device to monitor safety and proper coking, J Food Process Eng 36 (2012) 160–172.
[31] A.K.P.D. Savio, Characterization Protocol for Titanium Dioxide (anatase: Rutile) Use for Photocatalytic Applications, Mechanical Engineering Technology, University of Houston, Houston, 2011, pp. 158.
[32] U. Balachandran, N.G. Eror, Raman-spectra of titanium-dioxide, J Solid State Chem 42 (1982) 276–282.
[33] P.P. Lottici, D. Bersani, M. Braghini, A. Montenero, Raman-scattering characterization of gel-derived titania glass, J Mater Sci 28 (1993) 177–183.
[34] A.K.P.D. Savio, D. Starikov, A. Bensaoula, R. Pillai, L.L. de la Torre García, F.C. Robles Hernández, Tunable TiO_2 (anatase and rutile) materials manufactured by mechanical means, Ceram. Int. 38 (2012) 3529–3535.
[35] O. Frank, M. Zukalova, B. Laskova, J. Kurti, J. Koltai, L. Kavan, Raman spectra of titanium dioxide (anatase, rutile) with identified oxygen isotopes (16, 17, 18), Phys. Chem. Chem. Phys. 14 (2012) 14567–14572.
[36] D.T. Cromer, K. Herrington, The structures of anatase and rutile, J. Am. Chem. Soc. 77 (1955) 4708–4709.
[37] T.P. Ang, J.Y. Law, Y.F. Han, Preparation, Characterization of sulfur-doped nanosized TiO_2 and photocatalytic degradation of methylene blue under visible light, Catal Lett 139 (2010) 77–84.
[38] D.O. Scanlon, C.W. Dunnill, J. Buckeridge, S.A. Shevlin, A.J. Logsdail, S.M. Woodley, C.R. Catlow, M.J. Powell, R.G. Palgrave, I.P. Parkin, G.W. Watson, T.W. Keal, P. Sherwood, A. Walsh, A.A. Sokol, Band alignment of rutile and anatase TiO_2, Nat Mater 12 (2013) 798–801.
[39] Q. L. Liao, Z. Zhang, Z. Su, Y. Zhao, Y. Wang, X. Li, D. Lu, G. Wei, Q. Yu Feng, Efficient solar water-splitting using a nanocrystalline CoO photocatalyst, Nat Nanotechnol 9 (2014) 69–73.
[40] F.P. Koffyberg, Optical bandgaps and electron affinities of semiconducting Rh2O3(I) and Rh2O3(III), J Phys. Chem. Solids 53 (1992) 1285–1288.
[41] S.V. Dzyadevych, A.P. Soldatkin, J.M. Chovelon, Assessment of the toxicity of methyl parathion and its photodegradation products in water samples using conductometric enzyme biosensors, Anal. Chim. Acta 459 (2002) 33–41.
[42] Y.L. Zheng, D.L. Liu, H. Xu, Y.L. Zhong, Y.Z. Yuan, L. Xiong, W.X. Li, Biodegradation of p-nitrophenol by Pseudomonas aeruginosa HS-D38 and analysis of metabolites with HPLC-ESI/MS, Int. Biodeterior. Biodegrad. 63 (2009) 1125–1129.
[43] Y.L. Zheng, D.L. Liu, S.W. Liu, S.Y. Xu, Y.Z. Yuan, L. Xiong, Kinetics and mechanisms of p-nitrophenol biodegradation by Pseudomonas aeruginosa HS-D38, J. Environ. Sci. China 21 (2009) 1194–1199.
[44] W. Kitagawa, N. Kimura, Y. Kamagata, A novel p-nitrophenol degradation gene cluster from a gram-positive bacterium, Rhodococcus opacus SAO101, J. Bacteriol 186 (2004) 4894–4902.
[45] K.Y. C.T. Williams, C.G. Chen, M.J. Weaver Takoudis, Reduction kinetics of surface rhodium oxide by hydrogen and carbon monoxide at ambient gas pressures as probed by transient surface-enhanced raman spectroscopy, J. Phys. Chem. B 102 (1998) 4785–4794.
[46] M.C. Y.F. Wang, J.F. Hsieh, C.M. Yang Lee, Nonaqueous synthesis of CoO_x/TiO_2 nanocomposites showing high photocatalytic activity of hydrogen generation, Appl. Catal. B Environ. 142 (2013) 626–632.
[47] A. Bianco Prevot, C. Baiocchi, M.C. Brussino, E. Pramauro, P. Savarino, V. Augugliaro, G. Marcì, L. Palmisano, Photocatalytic degradation of acid blue 80 in aqueous solutions containing TiO_2 suspensions, Environ. Sci. Technol. 35 (2001) 971–976.